Fabrication and optical properties of transparent fine-grained Zn1.1Ga1.8Ge0.1O4 and Ni2+ (or Cr3+)-doped Zn1.1Ga1.8Ge0.1O4 spinel ceramics

J. Carreaud, J.-R. Duclère, Y. Launay, N. Tessier-Doyen, D.S. Smith, M Allix, V. Couderc, G. Delaizir, S. Chenu

Fabrication and optical properties of transparent fine-grained $Zn_{1.1}Ga_{1.8}Ge_{0.1}O_4$ and Ni^{2+} (or Cr^{3+})-doped $Zn_{1.1}Ga_{1.8}Ge_{0.1}O_4$ spinel ceramics.

Julie CARREAUD [a], Jean-René DUCLERE [a], Yann LAUNAY [a], Nicolas TESSIER-DOYEN [a], David S. Smith [a], Mathieu ALLIX [b], Vincent COUDERC [c], Gaëlle DELAIZIR [a], Sébastien CHENU [a,d]*

[a] *Institut de Recherche sur les Céramiques (IRCER), UMR CNRS 7315, Université de Limoges, Centre Européen de la Céramique, 87068 Limoges, France*

[b] Conditions Extrêmes et Matériaux : Haute Température et Irradiation (CEMHTI), UPR CNRS 3079, *CNRS UPR 3079, 45071 Orléans, France*

[c] *Xlim, UMR CNRS 7252, Université de Limoges, 87060 Limoges, France*

[d] *Rennes Institute of Chemical Sciences (ISCR), UMR CNRS 6226, University of Rennes, 35042 Rennes, France*

* Corresponding author - E-mail: sebastien.chenu@univ-rennes1.fr

Abstract:

For the first time, a $Zn_{1.1}Ga_{1.8}Ge_{0.1}O_4$ transparent spinel ceramic has been fully densified by spark plasma sintering. XRD measurements show that this ceramic is composed of a pure cubic spinel phase. SEM analysis revealed a homogeneous and dense microstructure with the average grain size being 200 ± 100 nm. The transmittance of these fine-grained ceramics reached 70% in the visible range and is very close to 80% at 2 µm, thus close to the T_{max} value deduced from the measurement of the refractive index. The ceramics exhibit excellent mechanical properties with a Young modulus of 222 GPa, a Vickers hardness of 14.25 GPa and a thermal conductivity of 7.3 $W.m^{-1}.K^{-1}$. By doping

with Cr^{3+} ions, transparent $Zn_{1.1}Ga_{1.8}Ge_{0.1}O_4$ ceramics present both a red luminescence and a long-lasting afterglow during several minutes. Moreover, a near infrared broadband emission at 1.3 µm is also achieved with Ni^{2+} ions.

Keywords:

Transparent spinel ceramics ; zinc gallate ($ZnGa_2O_4$) ; Spark Plasma Sintering (SPS) ; Optical properties ; Persistent luminescence

1 Introduction

Transparent polycrystalline ceramics are promising optical materials for laser media [1, 2], infrared domes [3, 4], electro-optic devices [5, 6], high refractive index lenses [7, 8], scintillators [9, 10], white light-emitting diodes [11, 12], or transparent armors [13, 14]. Compared to glasses, ceramics have stronger mechanical properties, greater thermal conductivity and excellent energy lasing effects due to their high crystallinity. They can also be high-performance/cheap substitutes for single crystals, which makes them suitable for photonic applications [15]. A major challenge in transparent ceramics technology has been the transparency loss caused by scattering. Most light-scattering sources arise from the ceramics' microstructure, such as pores, grain boundaries, grain size as well as the presence of impurities, secondary phases, and birefringence effects. Indeed, to achieve high transparent ceramics, porosity should be removed. Various strategies have been employed to minimize the residual porosity such as sintering process under high pressure (SPS, HP) or vacuum, but also by using sintering aids, and performing additional post-sintering heat treatments (HIP) [1, 15]. To overcome this bottleneck, some transparent oxide ceramics have been elaborated by full crystallization of dense bulk glasses [16]. In fact, it has been often reported that the porosity in transparent ceramics must remain smaller than 0.1% to reach photonic quality [17]. For these reasons, most research in the transparent ceramics field has been performed on materials with a cubic crystal structure such as: $Y_3Al_5O_{12}$ [1], Lu_2O_3 [18], $MgAl_2O_4$ [19], MgO [20], Lu_3NbO_7 [21],

$KNbTeO_6$ [22], CaF_2 [23], $CaLa_2S_4$ [3] and others. The reason for this lies in the inherent optical isotropy of cubic materials, while polycrystalline ceramics with lower symmetries exhibit optical anisotropy (i.e. birefringence), resulting in the creation of additional light-scattering sites at grain boundaries, due to the discontinuity in refractive index between grains with different orientations [24, 25]. Nevertheless, non-cubic transparent ceramics doped with magnetic ions have been reported by synthesis under a magnetic field during the sintering process to align grains and therefore limit the light scattering [5, 26]. Recently, Ikesue et al. have elaborated highly transparent alumina ceramics by annihilating birefringence effects present in this hexagonal ceramic thanks to a small amount of ZrO_2 additive leading to a grain boundary phase of nano-sized Al_2O_3-ZrO_2 composition (amorphous) formed at the grain boundary [27] .

In recent years, a strong interest has been also devoted to enlarge transparent ceramics family and to develop new optical ceramics [28, 29]. In particular, spinel transparent ceramics have received much attention from academia and industry sectors and widespread concern from researchers in many different fields because of their unique and interesting properties. Spinel oxide materials have a general AB_2O_4 formulation crystallizing in the cubic crystal system in which O^{2-} anions are arranged in a cubic close-packed lattice and the cations A and B occupying some or all of the octahedral and tetrahedral sites in the lattice [30]. $MgAl_2O_4$ is probably the most famous compound of this family and numerous studies have been dedicated to this ceramic [31, 32]. In the last decade, some studies have paved the way for the elaboration of novel transparent spinel ceramics such as $ZnAl_2O_4$ [33], $Mg_{0.55}Al_{2.36}O_{3.81}N_{0.19}$ [34], $MgGa_2O_4$ [35], $ZnGa_2O_4$ [36-40]. In addition, due to their tetrahedral and octahedral sites in its crystal structure, spinel is a promising host for divalent or/and trivalent cations such as transition metal ions: Co^{2+}, Ni^{2+} or Cr^{3+}. In 2021, for the first time, C. Mével et al. have reported, the elaboration of transparent $ZnGa_2O_4$ ceramics by spark plasma sintering, with red long-lasting luminescence when doped with Cr^{3+} [36]. Few months after, Liu et al. have prepared this same transparent ceramic by combining co-precipitation method and hot isostatic pressing [39]

and Wang et al. have fabricated this spinel ceramic by pressureless sintering and hot isostatic pressing [40]. For example, gallate spinel ceramics can exhibit different emission colors when doped with transition metal elements. With Ni^{2+}, a broadband infrared luminescence emission is observed around 1300 nm [35], while when doped with Cr^{3+}, it gives rise to a long red afterglow [36, 41]. Moreover, the long-lasting red luminescence properties of $ZnGa_2O_4$ ceramics can be significantly improved by germanium substitution, leading to a $Zn_{1+x}Ga_{2-2x}Ge_xO_4$ solid solution ($0 \leq x \leq 0.5$) [42]. To the best of our knowledge, this spinel solid solution has never been elaborated as a transparent ceramic but only as opaque ceramic for high-speed signal propagation applications [43].

In this work, we report, for the first time, the elaboration of transparent spinel ceramics, $Zn_{1.1}Ga_{1.8}Ge_{0.1}O_4$, by spark plasma sintering. The development of a suitable powder and the determination of appropriate conditions for powder densification are studied here. In the aim to enhance the powder sintering efficiency, both the effect of milling process and the impact of the calcination temperature on the morphology and the specific surface area of the as-prepared powders were evaluated. The optical transmittance of these spinel ceramics is measured in the visible and infrared ranges and correlated to structural and microstructural analyses. X-ray diffraction, ellipsometry and SEM observations were combined to understand optical properties. By doping these $Zn_{1.1}Ga_{1.8}Ge_{0.1}O_4$ transparent ceramics with metal transition ions such as Cr^{3+} and Ni^{2+}, optical active properties were induced. To gain a better understanding on these transparent spinel ceramics, their mechanical and thermal properties were also evaluated.

2 Experimental Section

2.1 Powder Synthesis

The powder precursors mixture was prepared using high energy ball milling of high purity precursors (ZnO - Aldrich 99.99 %, Ga_2O_3 - NanoShel 99.9 %, GeO_2 - Strem 99.999%), with a RETSCH EMAX grinding machine. The powder preparation is similar to the one used four our previous work

dealing with the elaboration of transparent $ZnGa_2O_4$ ceramic [36]. A 12 g batch was prepared in a stoichiometric molar ratio, using a two-step grinding protocol. The batch was poured in a 125 ml zirconia-coated jar filled with ethanol and 500 µm diameter zirconia grinding beads. A 20 minutes ball milling duration was processed at 1700 rpm. After the separation of beads and suspension using a 63 µm sieve and the drying of the obtained suspension, a second grinding was performed with 100 µm diameter zirconia beads using the same previous conditions. A powder:ball mass ratio of 1:6 was used in both cases. The separation of beads and precursor powder was made using a 32 µm sieve. The batch was dried overnight to remove ethanol and then fired at 800°C during 2 h to obtain the spinel compound and to also remove volatile compounds, hydroxyl and carbonate species. For doped samples, Cr_2O_3 (Alfa Aesar 99.97 %) or NiO (Strem 99.99%) were mixed with high energy ball milled precursors in an agate mortar with ethanol to ensure homogeneous repartition of dopant and finally fired at 800°C for 2 h. Both undoped and doped powders were then considered ready for spark plasma sintering.

2.2 SPS sintering.

A Spark Plasma Sintering equipment (Dr. Sinter 825 Syntex machine (Fuji FDC, Japan)) was used to densify the precursor mixture previously obtained. To do so, the powder was poured into an 8 mm diameter graphite die. For all the SPS attempts, the temperature was measured with a thermocouple positioned close to the sample, through the die. The sintering was performed under vacuum and no sintering aids or additives were used. The temperature was increased to 450°C within 5 minutes without applying pressure, except for contact. A 5 minutes dwell time was used while 100 MPa uniaxial pressure was applied. This pressure was kept constant until the end of the attempt. At the end of dwell time, the temperature was increased to higher temperature using a 50°C/min heating rate up to 850°C followed by a 5°C/min heating rate up to 900°C (950°C for Ni^{2+} doped samples). The experiment was stopped at this temperature and let to cool freely down to room temperature.

After this sintering step, the graphite foil was removed by polishing and a post annealing treatment in air was performed during 8h at 800°C to remove semiconducting effects [36].

2.3 Characterization methods

Particle size analysis was performed by laser diffraction granulometry (Malvern Mastersizer 2000). The powder was dispersed in ethanol by sonication for 5 min. Different granulometric analysis were realized on ZnO, Ga_2O_3 and GeO_2 precursors but also on ball-milled powders and also mixture of powders fired 2 hours at 800°C.

Powder X-ray diffraction (PXRD) data were recorded on a Bragg Brentano D8 Advance Bruker diffractometer (CuKα radiation) equipped with a LynxEye XE detector over an angular range of 10° < 2θ < 70° for phase identification and of 5°<2θ<140° using a 0.012 step size for structural refinements. These latter were performed using the Rietveld [44] method implemented in the JANA2006 software [45].

A Quanta 450 FEG Scanning Electron Microscope (SEM) was used to observe ceramic powders and to characterize the nanostructure of the ceramics. Element distributions of the ceramic samples were carried out using an Energy-dispersive spectrometer (EDS, SDD 30 mm^2 SamX). The bulk samples were optically mirror-polished prior to observations. The Feret diameter (D_f) was finally obtained by image analyses with ImageJ software [46]. The different steps of the image processing consisted in applying i) a threshold in grey level ii) a binarisation followed by iii) a segmentation to identify the border between all particles of the image. D_f corresponds to the diameter of the smallest circle in which each particle can fit.

The specific surface area (SSA) of the precursor -milled powder annealed at 800°C during 2 h was measured by BET (Brunauer, Emmett and Teller) using a Micromeritics ASAP 2020 equipment (USA).

The density of the samples was measured at room temperature using Archimedes' method with absolute alcohol as immersion fluid. The error in the determination of the density is ±0.02 $g.cm^{-3}$.

Optical transmission measurements were carried out with the ceramic (1.15mm of thickness) placed at normal incidence, within the 300 - 3300 nm range, using a Varian Cary 5000 spectrophotometer operated in a dual beam configuration and in the infrared range until 10 µm using a Thermo Scientific Nicolet 6700.

Concerning mechanical properties, the Vickers hardness (H_v) and fracture toughness (K_{1c}) were determined on mirror polished surfaces using a diamond Vickers indenter (Buelher MicroMet 6040) for a load of 100 g during 15 s. Elastic properties (Young's modulus E, shear modulus G, and Poisson's ratio ν) were determined by pulse echography technique operating in infinite medium mode at 10 MHz on an 8 mm diameter disc-shaped specimen exhibiting a thickness of 1.15 mm. In order to avoid the unexpected effect of the transducer near field, an alumina buffer has been placed between the transducer and tested specimens to determine accurately the propagation velocity of both longitudinal and shear ultrasonic waves.

Measurements of thermal diffusivity were made with a laboratory Laser flash set-up at room temperature. The accuracy for the value is generally within 3% related to measurements repeatability and evaluation of sample thickness. The sample discs were coated with the graphite aerosol spray on both faces prior to measurements, to enhance the absorption of the laser energy and improve the back face signal emission, therefore increasing the signal-to-noise ratio. Data were analyzed with the Degiovanni's method to take heat losses into account [47].

The chromatic dispersion of the linear refractive index n of the samples was accessed from ellipsometry measurements, performed using a Horiba Jobin-Yvon UVISEL Extended Range spectroscopic ellipsometer operated in the 200-850 nm range. The light spot size was fixed at 1 mm in diameter and the angle of incidence was selected at 62.5°, as it corresponds to a value very close to the Brewster angle.

Photoluminescence (PL), as well as long lasting phosphorescence (LLP) measurements, were carried out at room temperature, using a Fluorolog 3 spectrofluorimeter from Horiba Jobin-Yvon company.

In the case of transparent ceramics doped with Cr^{3+}, steady state fluorescence emission spectra were recorded in the 600 – 800 nm range, with a data step fixed at 0.25 nm, with a 0.5 s acquisition time and a 0.5 nm emission slit size. LLP data were collected 10 s after the excitation stoppage and then with time interval steps of 10 s. The afterglow intensity is normalized at 1 by using the value measured 10 s after the excitation stoppage, thus allowing the comparison of the rate of decay between different curves. In the case of Ni^{2+}-doped ceramics, steady state fluorescence data were collected in the NIR range, between 1000 and 1650 nm, using an increment step fixed at 1 nm, with a 0.5 s acquisition time and a 2 nm emission slit size.

3 Results and discussion

Stoichiometric amounts of commercial ZnO, Ga_2O_3 and GeO_2 powders were finely ground in ethanol by high-energy ball milling process in zirconia media during 20 minutes with beads of 500 µm in diameter. The second grinding step has been realized with beads in 100 µm of diameter during 20 min. at 1700 rpm. The obtained slurry was sieved to remove zirconia balls, dried in air to remove liquid ethanol and then calcined at 800°C for 2 hours to crystallize the desired spinel compound, $Zn_{1.1}Ga_{1.8}Ge_{0.1}O_4$ [42].

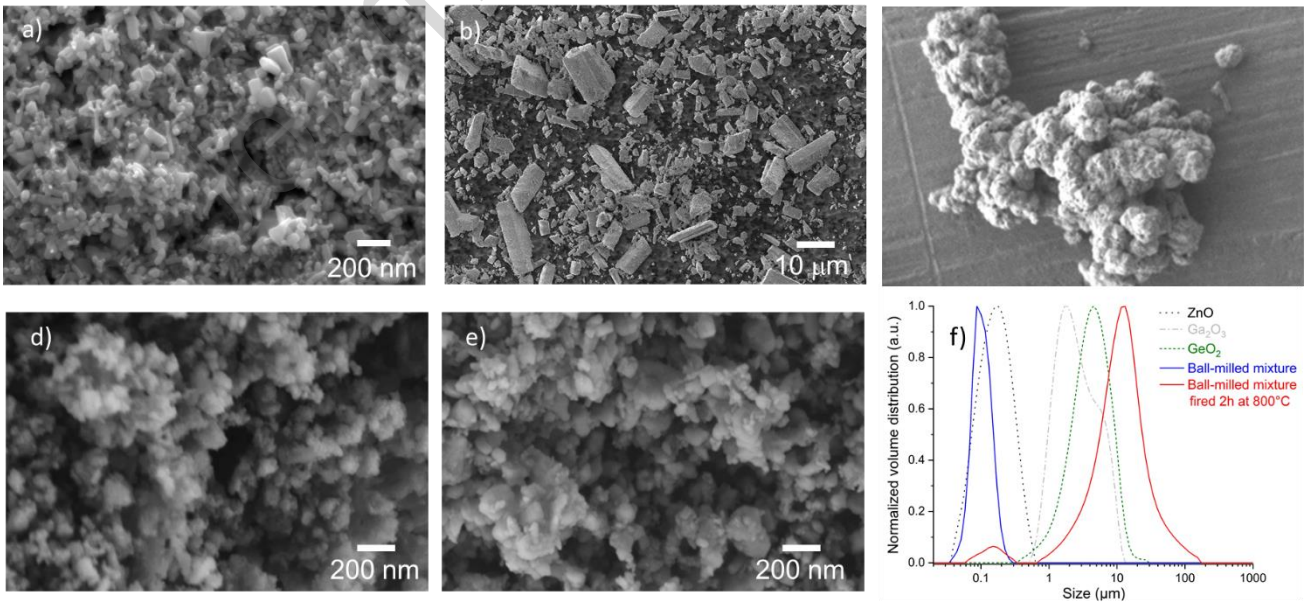

Figure 1: SEM observations of: raw precursors (a) ZnO, b) Ga_2O_3 and c) GeO_2), d) ball-milled mixture after the two grinding steps at 1700 rpm, e) ball-milled mixture fired during 2 hours at 800°C. f) Particle size

distribution of precursors (dashed curves with ZnO (black), Ga_2O_3 (grey) and GeO_2 (green)), ball-milled mixture (blue) and ball-milled mixture fired for 2 hours at 800°C (red).

SEM observations of raw precursors, milled mixtures and ceramic powder synthesized at 800°C are presented in Figure 1. One can observe that Ga_2O_3 and GeO_2 (Figure 1-b and 1-c respectively) are strongly agglomerated with a micrometric size distribution while ZnO (Figure 1-a) is a monodisperse nanometric powder. As illustrated in Figure 1-d), the two-step grinding process allows to ensure homogeneity in morphology and a uniform particle size distribution centered on 90 nm is obtained, as presented in Figure 1-f (blue curve). Therefore, this grinding process makes it possible to obtain precursors with a narrow particle size distribution and thus to get a comparable chemical reactivity to form the desired spinel compound during the firing step. The calcination of ball-milled mixture at 800°C during two hours has limited impact on the morphology of as synthetized ceramic powders (Figure 1-e) and no considerable grain growth is observed since some ceramic particles exhibit an average size centered on ~150 nm. Nevertheless, one can note that the granulometric distribution of this fired powder is bimodal with a second population corresponding to aggregates of ~12 µm, as shown in Figure 1-f (red curve). While this heat treatment occurs a slight agglomeration of this powder, this effect is limited as since the particle size curves, plotted in number, show that a very large number of these particles have a size centered around ~80 nm (Figure SI-1). The BET surface area of the ball-milled powder calcinated at 800°C was 14.74 m^2/g. As shown in Figure 2, after the ball milling process, only raw materials (ZnO, Ga_2O_3 and GeO_2) are identified by XRD, attesting no reaction between precursors and ethanol. As expected, these milled powders were white. Moreover, there was no evidence of the presence of zirconia impurities within the accuracy of X-ray diffraction technique. The calcination of this milled mixture at 800°C during 2 hours allows us to obtain a single crystalline phase consistent with a cubic spinel $Zn_{1.1}Ga_{1.8}Ge_{0.1}O_4$ phase [42]. A very minor peak could be detected (see unfilled triangle on the enlargement of Figure 2-b) corresponding to ZnO precursor and indicating that the solid-state reaction is slightly incomplete at this temperature. A

small quantity of gallium oxide is also probably present in this powder but XRD measurements do not allow to detect it because of an important overlapping of diffraction peaks between Ga_2O_3 and $Zn_{1.1}Ga_{1.8}Ge_{0.1}O_4$ phases. One can note that the ball milling process decreases considerably the temperature of reaction compared to the solid state reaction of micrometric precursors as published by Allix et al. [42].

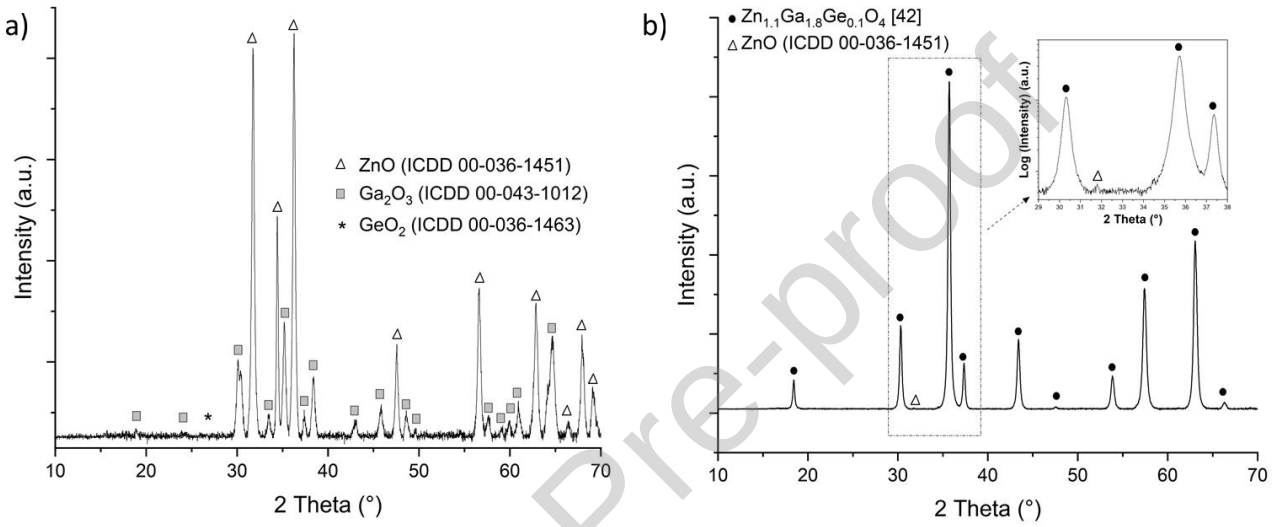

Figure 2: XRD patterns of a) ball-milled mixture after the two grinding steps at 1700 rpm and b) ceramic powders after a calcination process during 2 hours at 800°C. The inset of b) corresponds to an enlargement of the same data.

The as-prepared ceramic powder was subsequently loaded in a graphite die of 8 mm in diameter and sintered with a spark plasma sintering equipment (Dr. Sinter 825 Syntex) under a maximum pressure of 100 MPa while seeking to obtain a new transparent spinel ceramic. A two-step sintering profile was applied and the complete SPS sintering cycle (Figure 3) is relatively short, less than 40 minutes, with an apparent densification starting near 700°C and complete at around 900°C. One can note that a low heating rate (5°C/min.) was used from 850°C in order to limit residual porosity and pores size without significant grain growth as shown by Morita et al. [48] for $MgAl_2O_4$ ceramics. This SPS densification method is time and energy saving compared to conventional sintering such as vacuum sintering which necessitates several hours at higher temperatures (>1500°C) [15, 33]. It is well-

known that the external field of electric current and pressure enables rapid heating, short sintering times and densification at low temperatures [49].

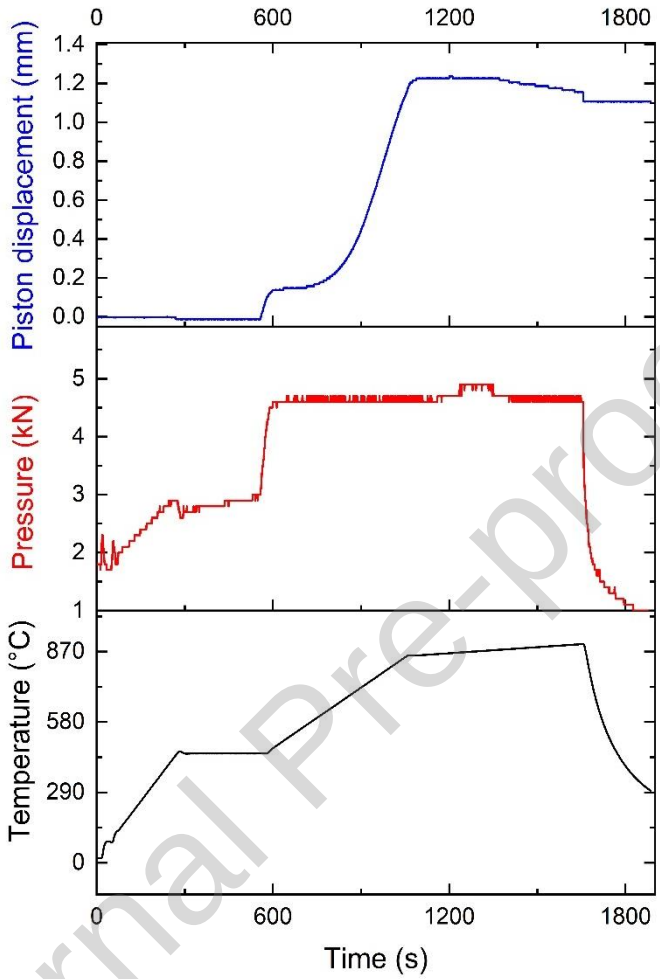

Figure 3: Typical sintering profiles including temperature, pressure and piston displacement as function of time during SPS cycle.

The visual appearance of the resulting polished $Zn_{1.1}Ga_{1.8}Ge_{0.1}O_4$ ceramic (thickness of 1.15mm) is presented in

Figure 4. The ceramic appears transparent in the visible range and the text remains perfectly readable through the pellet despite the fact that the ceramic is placed perpendicular to it. Therefore, with this level of transparency, this ceramic is expected to be a dense material [15]. These observations show that it is possible to develop dense and transparent zinc gallate germanate spinel ceramics by SPS. One can note that the edge of this spinel ceramic is black, as a consequence of the carbon diffusion occurring during the SPS process, due to the use of a graphite foil; the latter was removed afterwards

by polishing. This radial diffusion is clearly visible in the photographs taken of the undoped $Zn_{1.1}Ga_{1.8}Ge_{0.1}O_4$ ceramic (blue) and ceramics doped with 0.1% of Cr^{3+} (red) and 0.05% Ni^{2+} (dashed black) (Figure SI-6). The same trend is observed by Zhang et al. during the sintering of $MgGa_2O_4$ ceramics [35]. Thus, for these 1.15 mm thick samples, the optical transmission was spectra thus systematically measured through the central area as depicted in

Figure 4.

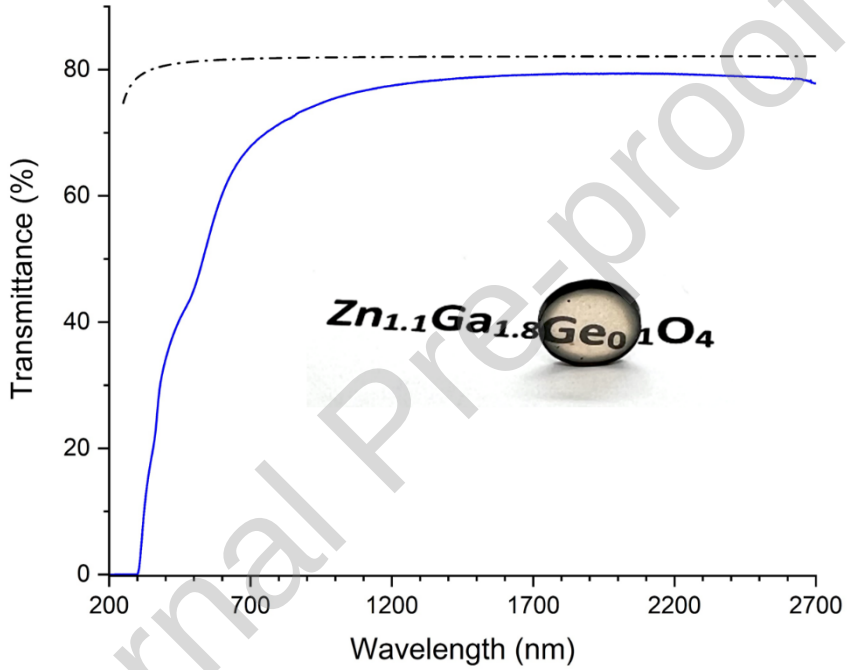

Figure 4: Optical transmittance spectrum of fine-grained $Zn_{1.1}Ga_{1.8}Ge_{0.1}O_4$ spinel ceramic with a thickness of 1.15 mm. The dashed line corresponds to the maximum transmittance of this material, deduced from the chromatic dispersion of the refractive index measured by spectroscopic ellipsometry (Figure SI-3). In inset, the photograph of this $Zn_{1.1}Ga_{1.8}Ge_{0.1}O_4$ spinel ceramic with a thickness of 1.15 mm and a diameter of 8 mm.

In the visible range, this spinel ceramic has a good transmittance with 53% at 550 µm and 70% at 800 nm. It is important to highlight that the air annealing treatment (at 800°C during 8 hours) realized on ceramics after SPS densification does not reduce the average transmission level in the visible range contrary to observations previously reported on $MgGa_2O_4$ [35], which attest that no growth of pore size occurs during this annealing. Nevertheless, air-annealing treatment allows to

reach maximum of infrared transmission by removing semiconducting effects as observed for SPS densified $ZnGa_2O_4$ ceramics [36]. The maximum of transmittance is reached in the near infrared region, around 2 µm, with a value of 79.5 %. This value is close to the maximum theoretical value for the transmission, which is calculated to be slightly above 82.1 %, based on the chromatic dependence of the refractive index measured on the same sample by spectroscopic ellipsometry (Figure SI-3). Indeed, using the well-known Sellmeier dispersion expression, it was possible to correctly fit the refractive index data (Figure SI-3) in the 250 - 820 nm wavelength range (the quality of the fit is reflected by a r^2 value equal to 0.9997). This allowed us extracting first the refractive index value at infinite wavelength (where there is no more chromatic dispersion), which was found close to 1.912. Moreover, by taking into account the contribution of the light reflections at the two air/ceramic interfaces, it is possible to express the following relationship between n and T_{max} (the maximum transmission coefficient): $T_{max} = 2n(\lambda)/(n(\lambda)^2 + 1)$. The chromaticity of the refractive index is then considered, as well as the absorption coefficient which is set equal to 0 cm^{-1}. And finally, injecting the above refractive index value of 1.912 ± 0.004 at infinite wavelength into the previous equation leads to derive a maximum theoretical value for the transmission estimated to be ~ 82.1 %. Furthermore, the optical window of this material extends from 0.3 up to 9 µm (Figure SI-4). It can be noted that the multiphonon cut-off wavelength of $Zn_{1.1}Ga_{1.8}Ge_{0.1}O_4$ ceramic is similar to that of $ZnGa_2O_4$ ceramic [36] since zinc, gallium and germanium have close molar mass (i.e. Ga is replaced by Zn and Ge).

As illustrated in Figure 5-a, SEM observations reveal a typical nanostructure of dense ceramic obtained by powder densification. The average grain size distribution is plotted in Figure 5-b and is around 200 ± 100 nm with relatively uniform distribution. Few black dots are visible in SEM image, attesting that this fine grained spinel ceramic presents few intergranular porosities, which could be source of light scattering and slightly reduce its transparency [24]. The average diameter of these pores is around 20 nm, so their detrimental effect on the light transmission is limited due to their

relative small size (less than one tens of the incident wavelength) according to the Rayleigh scattering law [17]. Moreover, EDS mapping images (Figure SI-2) reveal a homogeneous distribution of Zn, Ga and Ge elements in this spinel ceramics. It is noteworthy that the Ga/Zn ratio of this transparent ceramic was measured at 1.642 which was very close to the theoretical ratio (i.e. 1.640) and Ge/Ga ratio is estimated to 0.050 for a theoretical value of 0.056, as supported by the EDS patterns of the different selected points.

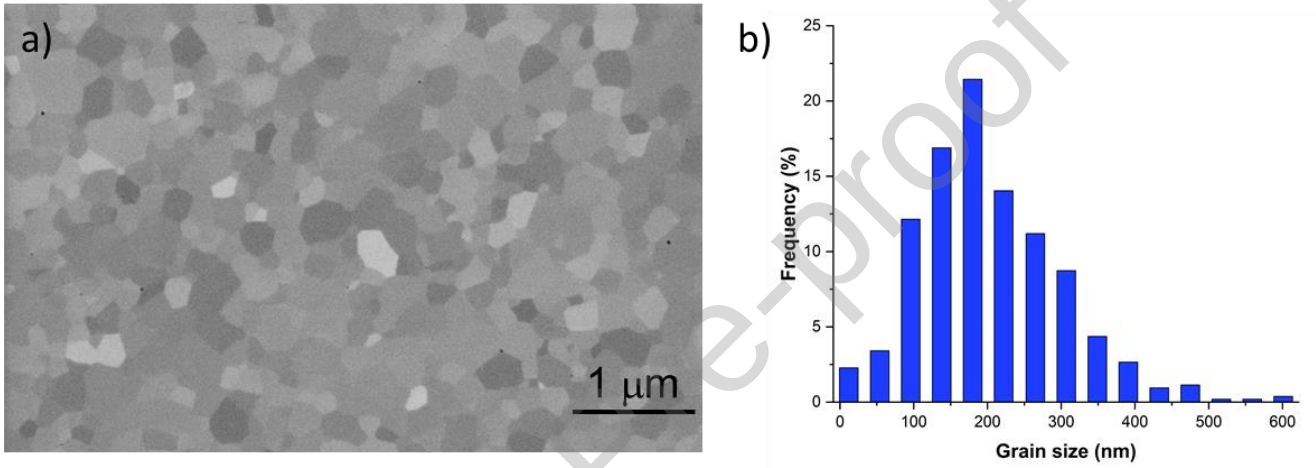

Figure 5: a) Microstructure of transparent $Zn_{1.1}Ga_{1.8}Ge_{0.1}O_4$ ceramic densified at 900°C by SPS. b) Corresponding grain size distribution.

Figure 6 shows phase identification of transparent $Zn_{1.1}Ga_{1.8}Ge_{0.1}O_4$ ceramic realized by XRD measurements and Rietveld refinement. This ceramic is composed of a pure cubic spinel $Zn_{1.1}Ga_{1.8}Ge_{0.1}O_4$ phase [42] and no secondary crystalline phase was detected, within the accuracy of X-ray diffraction technique. After densification process (SPS + post annealing in air), trace of precursors was not detected attesting that the formation $Zn_{1.1}Ga_{1.8}Ge_{0.1}O_4$ phase was complete. The Rietveld refinement, with agreement factors wRP = 2.97 %, Rp = 2.17 % and GOF = 2.96, converged easily and the cell parameter a = 8.33710 (2)Å is very close to the literature (8.3336 Å) [42]. The theoretical value of density (determined by XRD) for this material was estimated to 6.1590 $g.cm^{-3}$. Experimentally, a density of 6.13 $g.cm^{-3}$ was measured which corresponds to a relative density of 99.5 ± 0.4 %. This density value measured by Archimedes technique is not enough

accurate to discuss the optical transmittance of these ceramics. Nevertheless, the slight decrease of transmittance compared to the theoretical transmittance is probably linked to the presence of a small number of closed pores (i.e. light scattering sources [24]), observed by SEM at the grain boundary junctions of these ceramics.

For doped ceramics, their transmittance is slightly lower than undoped samples probably due to a larger number of pores. For possible laser applications, HIP post-treatment could be realized on these samples to remove this closed porosity and to reach theoretical transmittance value [15].

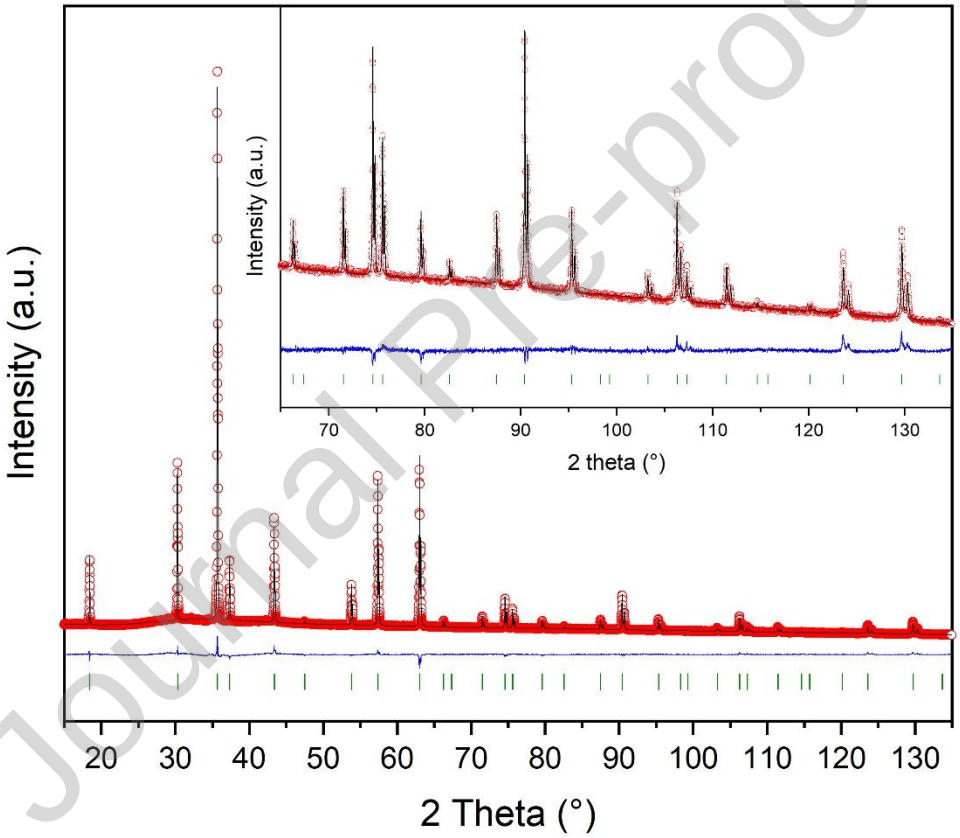

Figure 6: XRD patterns and Rietveld refinement of fine-grained $Zn_{1.1}Ga_{1.8}Ge_{0.1}O_4$ transparent ceramic sintered by SPS at 900°C and post-treated treated in air during 8h at 800°C. Data has been recorded from a ground transparent ceramic. Black circles, red and blue solid lines, vertical green ticks correspond to experimental data, simulated diagram, difference curve and indexations, respectively. The inset corresponds to an enlargement of the same refined data. Reliability factors are wRP = 2.97 %, Rp = 2.17 % and GOF = 2.96.

To gain a better understanding on these transparent $Zn_{1.1}Ga_{1.8}Ge_{0.1}O_4$ ceramics, their mechanical and thermal properties were evaluated and summarized in Table 1.

Table 1: Mechanical and thermal properties of transparent spinel $Zn_{1.1}Ga_{1.8}Ge_{0.1}O_4$ ceramics compared to $ZnGa_2O_4$ ceramics [40].

Samples	$ZnGa_2O_4$ [40]	$Zn_{1.1}Ga_{1.8}Ge_{0.1}O_4$
Young Modulus, E (GPa)	227.04	222
Shear Modulus, G (GPa)	/	87
Poisson ratio, υ	/	0.27
Vickers Hardness, H_v (GPa)	10.56	14.25
Fracture toughness, K_{1c} ($MPa.m^{-1/2}$)	1.83	1.66
Thermal conductivity ($W.m^{-1}.K^{-1}$)	19.46	7.3
Average grain size (nm)	3200	200

Young's and shear modulus so as Poisson's ratio determined by ultrasonic method are respectively equal to 222 GPa, 87 GPa and 0.27. These values are well consistent with the values of $ZnGa_2O_4$ ceramics measured by Wang et al. [40]. The compositions are relatively close, which explain why these mechanical values are similar. The hardness of $Zn_{1.1}Ga_{1.8}Ge_{0.1}O_4$ ceramic is around 14.25 GPa which is 35% higher than $ZnGa_2O_4$ ceramics [40]. This increase is directly linked to the microstructure of ceramics. Indeed, in this work, these fine-grained $Zn_{1.1}Ga_{1.8}Ge_{0.1}O_4$ ceramics have an average grain size around 200 nm while Wang et al. [40] have micrometric grains eight times larger (i.e. 3200nm). It is well known that reducing grain size is the key strategy to increase the mechanical performance of ceramic materials [15]. Furthermore, our transparent ceramic possess a thermal conductivity of 7.3 $W.m^{-1}.K^{-1}$ at room temperature, which is much less than 19.5 $W.m^{-1}.K^{-1}$ for $ZnGa_2O_4$ ceramics. Though variation in the intrinsic grain conductivity, due to the incorporation of Ge, cannot be excluded, this reduction of thermal conductivity for the fine-grained ceramic could be largely attributed to the role of grain boundary thermal resistance. Given a physically reasonable

value of approximately 10^{-8} $m^2.W.K^{-1}$ per grain boundary, the change of grain size from 3.2 microns to 0.2 microns reduces the conductivity from 19 $W.m^{-1}.K^{-1}$ to 10 $W.m^{-1}.K^{-1}$ [15, 50].

The active optical properties of these new transparent ceramics have been also evaluated in both visible and near infrared ranges. Therefore, Cr^{3+} and Ni^{2+} doped ceramics have been prepared and densified by SPS. $ZnGa_2O_4$ spinel ceramics doped with Cr^{3+} are famous red emitters and notably present a strong red long-lasting luminescence at 696 nm [51] which was reported to be neatly enhanced in $Zn_{1+x}Ga_{2-2x}Ge_xO_4$ ceramics [42]. As illustrated in Figure 7-a, photoluminescence measurements conducted on two different Cr^{3+}-doped transparent $Zn_{1.1}Ga_{1.8}Ge_{0.1}O_4$ ceramics, which have undergone different post annealing treatments in air and which present different Cr levels, display effectively a typical red luminescence, which is visually highlighted in Figure 7-d. under UV excitation. These emission spectra are composed of different features:

- several narrow lines (R1 and R2) that constitute recognizable features from Cr^{3+} ions located in a strong field with octahedral coordination [51].

- the so-called N2 line, centered at ~ 694 nm, established to originate from other Cr^{3+} ions with a perturbed environment which is actually distorted by an anti-site defect, located in the first cationic neighbors of such Cr^{3+} ions [52-54].

- the N1 line is also visible at ~ 690 nm. The explanations for such feature appear controversial in the literature. Indeed, the N1 line was either attributed to a Cr^{3+} - Zn_i pair (Zn_i = interstitial Zn), according to Zhang *et al*. [52] or to a Cr^{3+} - V_{Zn} pair (V_{Zn} = Zn vacancy), based on the work of Nie *et al*. [55].

Interestingly, we have compared the PL emission issued from these two Cr^{3+}-doped $Zn_{1.1}Ga_{1.8}Ge_{0.1}O_4$ ceramics with that of Cr^{3+}-doped $ZnGa_2O_4$ ceramics (same excitation wavelength fixed at ~ 410 nm). The spectral differences are blatant:

- first, the relative intensity of the R lines is by far stronger in the case of the $ZnGa_2O_4$ ceramic, or in other words, the N2 line relative intensity is reinforced for the $Zn_{1.1}Ga_{1.8}Ge_{0.1}O_4$ ceramics. Such

observation would then concord with the strong enhancement of the LLP observed in $Zn_{1+x}Ga_{2-2x}Ge_xO_4$ ceramics [42], as it is well-known that the N2 line (*i.e*. Cr^{3+} ions at distorted octahedral sites) accounts for the delayed emission [51].

- then, it can be seen that the relative intensity of the N1 line is neatly enhanced in the case of the $Zn_{1.1}Ga_{1.8}Ge_{0.1}O_4$ ceramic. Considering the over-stoichiometric Zn composition in $Zn_{1.1}Ga_{1.8}Ge_{0.1}O_4$, our experimental observations seem to match better the hypothesis of the formation of a Cr^{3+} - Zn_i pair, defended by Zhang *et al*. [52].

Thus, from Figure 7-a, one clearly notices that the main spectral modifications are related to the partial substitution of Ga by Ge and Zn, whereas the change of the post annealing temperature and time or of the tested Cr level seems to have a more reduced impact on the spectral shape. Besides, the corresponding excitation spectrum associated to the light emission at 694 nm is given in Figure SI-5 where three different excitation bands can be clearly evidenced at roughly 307, 409 and 550 nm. The most intense excitation band corresponds to the central one, explaining why we selected an excitation wavelength at ~ 410 nm (the spectral position slightly differs from one sample to another) to record the different emission spectra displayed at Figure 7-a. In addition, the use of a visible excitation (rather than UV) is preferable in order to irradiate a larger volume of the samples. Furthermore, one can note that this strong red emission is observed in Cr^{3+}-doped $Zn_{1.1}Ga_{1.8}Ge_{0.1}O_4$ ceramic while a blue emission is observed for undoped sample (Figure 7-d). This blue emission is well known for $ZnGa_2O_4$ materials and could be related to the self-activation center of the octahedral Ga-O group in the spinel lattices and the Ga^{3+} ions combine with UV-generated free electrons produced in oxygen vacancies [56, 57]. Moreover, Zhang et al. have also reported that carbon impurities in zirconia powders could tune luminescence emission towards blue colors [58]. So, the presence of carbon contamination could also influence this blue emission in undoped $Zn_{1.1}Ga_{1.8}Ge_{0.1}O_4$ ceramic.

The good optical quality is finally attested by the pictures of our ceramics taken under the sun light illumination (Figure 7-c). For more information, the transmittance of these ceramics has been measured and compared for undoped and doped ceramics as presented in Figure SI-6. Moreover, this transparent Cr^{3+}-doped ceramic exhibits red long-lasting luminescence when the UV excitation is stopped, even after 5 min: this effect is particularly visible in Figure 7-e. The normalized afterglow intensity was also recorded for λ_{em} = 694 nm (N2 line) as a function of time (Figure 7-b). Such afterglow intensity reveals that this red emission is still considerably higher than the noise background (close shutter) even a quarter of an hour after excitation stoppage.

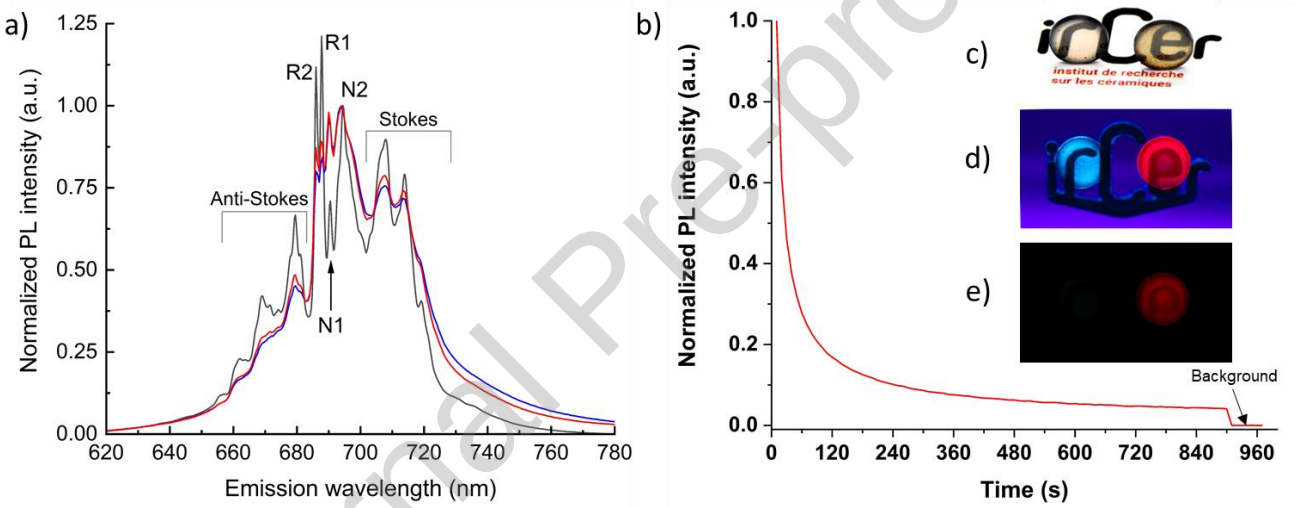

Figure 7: a) Comparison of fluorescence spectra of $ZnGa_2O_4$ doped with 0.2% Cr^{3+} and treated 4h at 800°C (grey curve), $Zn_{1.1}Ga_{1.8}Ge_{0.1}O_4$ doped with 0.2% Cr^{3+} and treated 4h at 800°C (blue curve) and $Zn_{1.1}Ga_{1.8}Ge_{0.1}O_4$ doped with 0.1% Cr^{3+} and treated 8h at 900°C (red curve). The normalization to 1 is made on the N2 line, after background removal. b) Long lasting luminescence spectra of 0.1% Cr^{3+}-doped $Zn_{1.1}Ga_{1.8}Ge_{0.1}O_4$ ceramics densified by spark plasma sintering and post-SPS treated at 900°C during 8 h under air. The excitation wavelength (λ_{exc}) used was 410 nm. Photography of undoped (left) and Cr^{3+}-doped (right) $Zn_{1.1}Ga_{1.8}Ge_{0.1}O_4$ ceramics have been recorded under (c) sun light, (d) UV excitation (luminescence at 254 nm) and (e) after 5 minutes excitation stoppage (long-lasting luminescence). These ceramics have a thickness of 1.15 mm.

Ni^{2+}-doped $Zn_{1.1}Ga_{1.8}Ge_{0.1}O_4$ ceramic have been also developed since this transition metal ion could be used in zing gallate spinel as a lasing ion between 1100 and 1700nm for broadband tunable near-infrared light sources [59, 60]. The photoluminescence spectrum of 0.05% Ni^{2+}: $Zn_{1.1}Ga_{1.8}Ge_{0.1}O_4$ transparent ceramic was obtained with a 294 nm excitation, as shown in Figure 8.

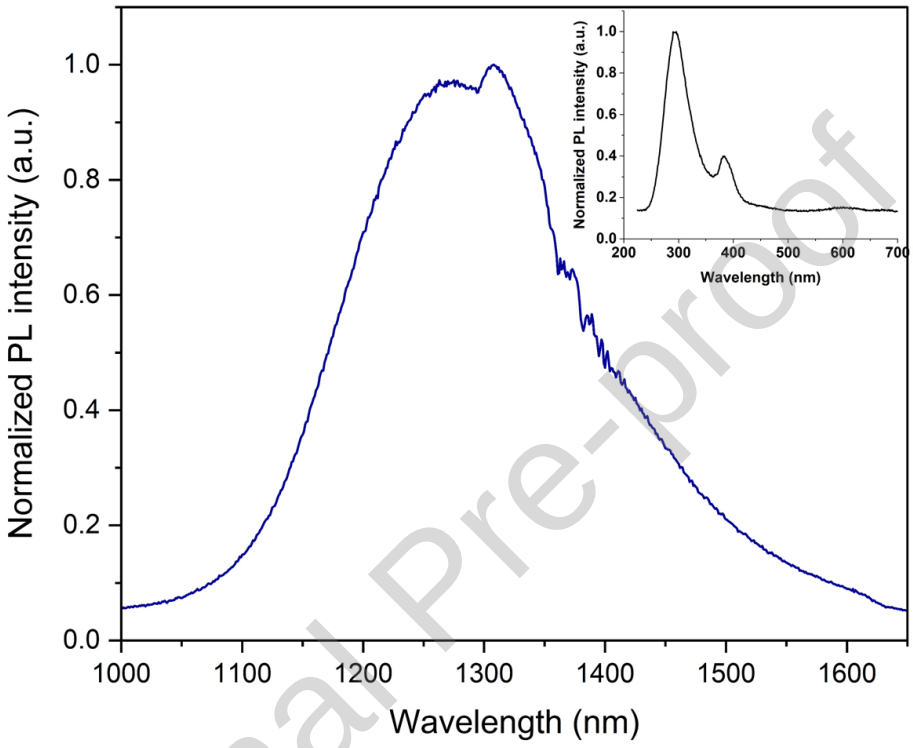

Figure 8: Normalized photoluminescence intensity collected for 0.05 % Ni^{2+}-doped transparent $Zn_{1.1}Ga_{1.8}Ge_{0.1}O_4$ ceramic, for λ_{exc} = 294nm. The corresponding excitation spectrum is represented in the inset.

As expected, a broad near infrared emission is observed in the near-infrared spectral region between 1050 and 1650nm. The full-width half-maximum obtained from a Gaussian fit was equal to 235 nm. This broad emission is composed of two peaks centered at 1276 nm and 1310 nm which are related to $^3T_2(^3F) \rightarrow {}^3A_2(^3F)$ transition of octahedrally coordinated Ni^{2+} ions. As explained by Jin et al. [61], the peak at 1310 nm can be assigned to the emission of the Ni^{2+} ions normally occupying the Ga^{3+} ions sites and the other one at 1276 nm can be assigned to the emission of the Ni^{2+} ions that are adjacent to anti-site defects. Therefore, zinc germanate gallate spinel transparent ceramics could be

promising solid-state laser materials in the eye-safe region in the 1.1 - 1.5 µm range provided that the Ni^{2+} concentration is increased sufficiently to allow sufficient amplification and consequently lasing [62]. Finally, succeeding in doping $Zn_{1.1}Ga_{1.8}Ge_{0.1}O_4$ with a transition metal ion different from Cr^{3+} also prove the versatility of these new transparent ceramics in this regard.

4 Conclusions

In this study, transparent $Zn_{1.1}Ga_{1.8}Ge_{0.1}O_4$ ceramics have been densified at 900°C by spark plasma sintering using high energy ball-milled powders. A fine-grained microstructure with an average grain size of 200 nm is obtained and conferred to this material excellent mechanical and thermal properties such as a Young's modulus value of 222 GPa, a Vickers hardness of 14.25 GPa and a thermal conductivity of 7.3 $W.m^{-1}.K^{-1}$. These as-prepared ceramics are composed of a pure cubic spinel $Zn_{1.1}Ga_{1.8}Ge_{0.1}O_4$ phase with a dense microstructure which allow reaching a high level of transparency in both visible and infrared ranges (around 70 % at 800 nm and 80 % at 2 µm for a thickness of 1.15mm). The corresponding optical window extends from 0.3 µm to 9 µm with a refractive index of 1.912 at infinite wavelength. Active optical properties have been also evaluated and these spinel ceramics can present both an intense red luminescence and a long-lasting afterglow during several minutes when doped with Cr^{3+} ions. By doping these spinel ceramics with NiO, a broad emission is observed in the near-infrared spectral region between 1050 and 1650nm, with full width at half-maximum of 235 nm. The tunable emissions, excellent optical and thermomechanical properties make $Zn_{1.1}Ga_{1.8}Ge_{0.1}O_4$ ceramics promising candidates for laser emission sources.

Acknowledgements

This work was supported by institutional grants from the LabEX SigmaLim (ANR-10-LABX-0074-01). This project is also co-funded by the European Union, the Region Centre Val de Loire, and the French minister of research (MESRI-DRRT). Europe is committed to the Centre-Val de Loire region with the European regional development fund (ERDF). The authors would like to thank the MON

ECOLE project (AAPR2021-2020-11934110) for its financial support and Benoit Naït-Ali (lecturer at IRCER) for his experimental assistance on thermal conductivity characterizations.

Declaration of competing interest

The authors have no competing interests to declare that are relevant to the content of this article.

Electronic Supplementary Material (ESM) (if applicable)

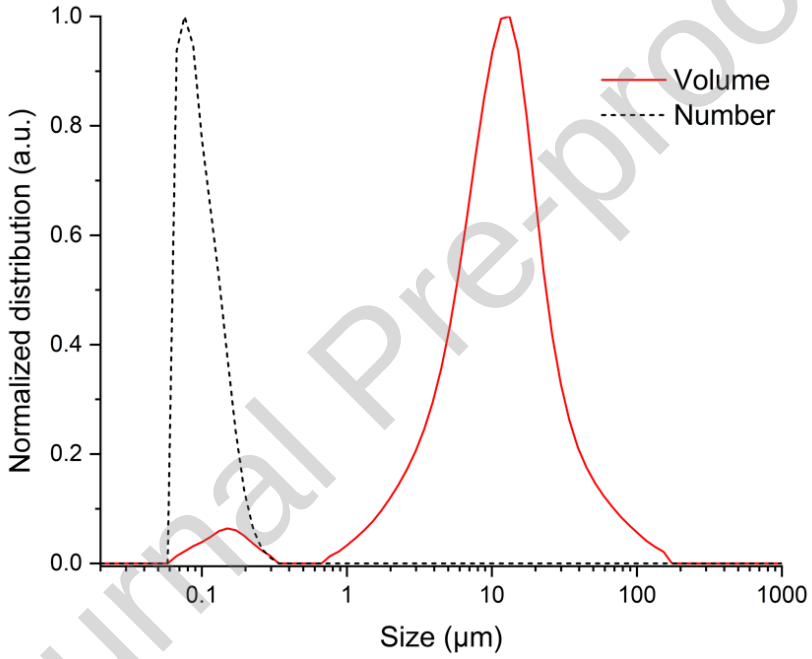

Figure SI-1: Comparison of particle size distribution (volume versus number) of ball-milled mixture fired 2 hours at 800°C.

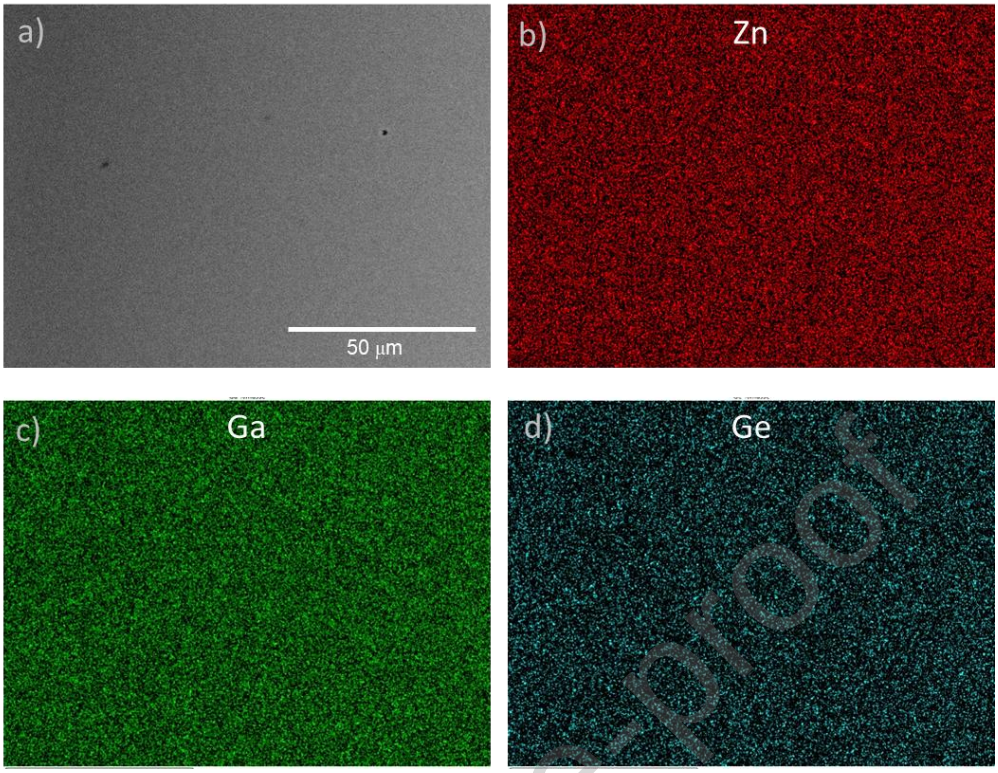

Figure SI-2: (a) SEM image of $Zn_{1.1}Ga_{1.8}Ge_{0.1}O_4$ transparent ceramic. (b-d) EDS mapping images of the same area.

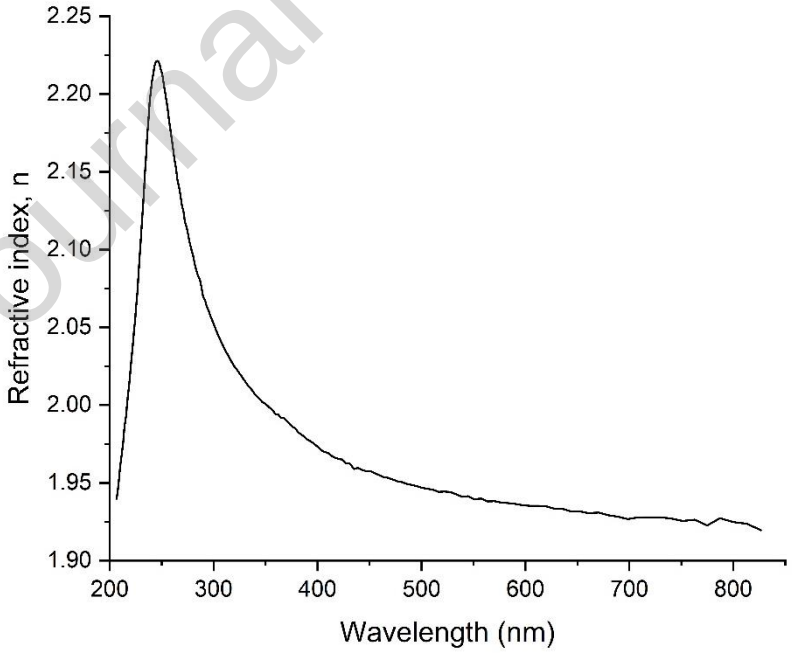

Figure SI-3: Refractive index n of $Zn_{1.1}Ga_{1.8}Ge_{0.1}O_4$ transparent ceramic as a function of wavelength.

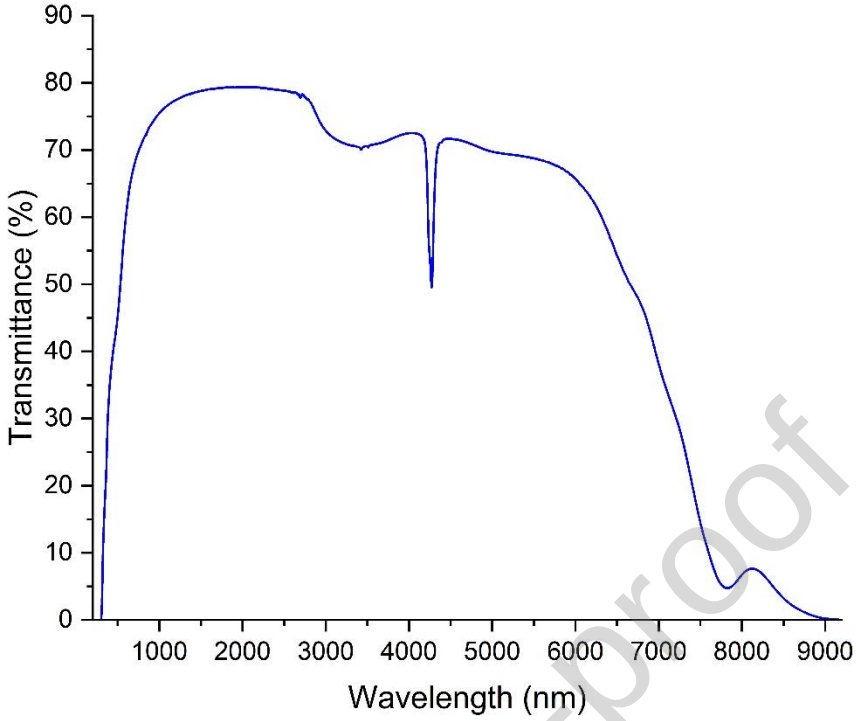

Figure SI-4: Optical transmittance spectrum of fine-grained $Zn_{1.1}Ga_{1.8}Ge_{0.1}O_4$ spinel ceramic with a thickness of 1.15mm. The sharp absorption band around 4.27 µm is observed and could be related to trapped CO_2 gazes [36] while the broad one located around 3 µm is due to the presence of free hydroxyl groups [63] probably exacerbated by the milling procedure conducted in ethanol media.

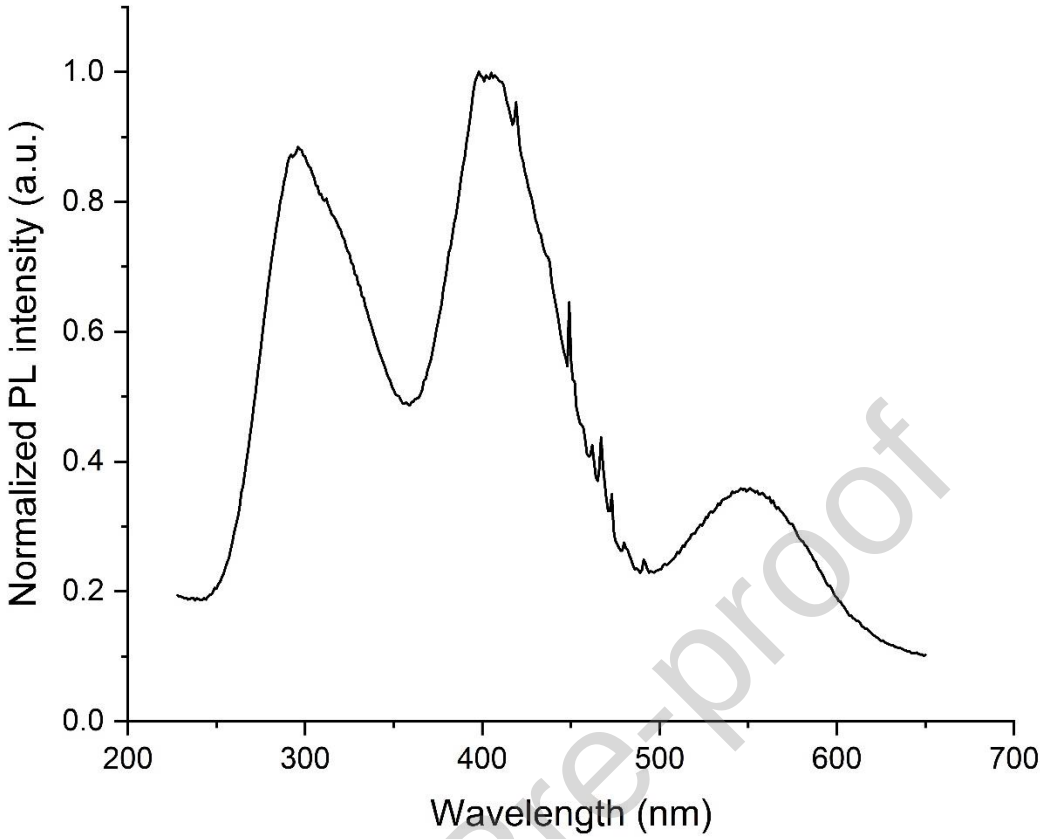

Figure SI-5: Excitation spectrum of $Zn_{1.1}Ga_{1.8}Ge_{0.1}O_4$ transparent ceramic doped with 0.1% Cr^{3+} associated to the emission at 694 nm (N2 line). Please note that the observed sharp lines arise from the Xe lamp source; these are typical artifacts, frequently met in the 400 – 500 nm spectral range, despite the use of a FGL400 Long Pass Filter on the emission side.

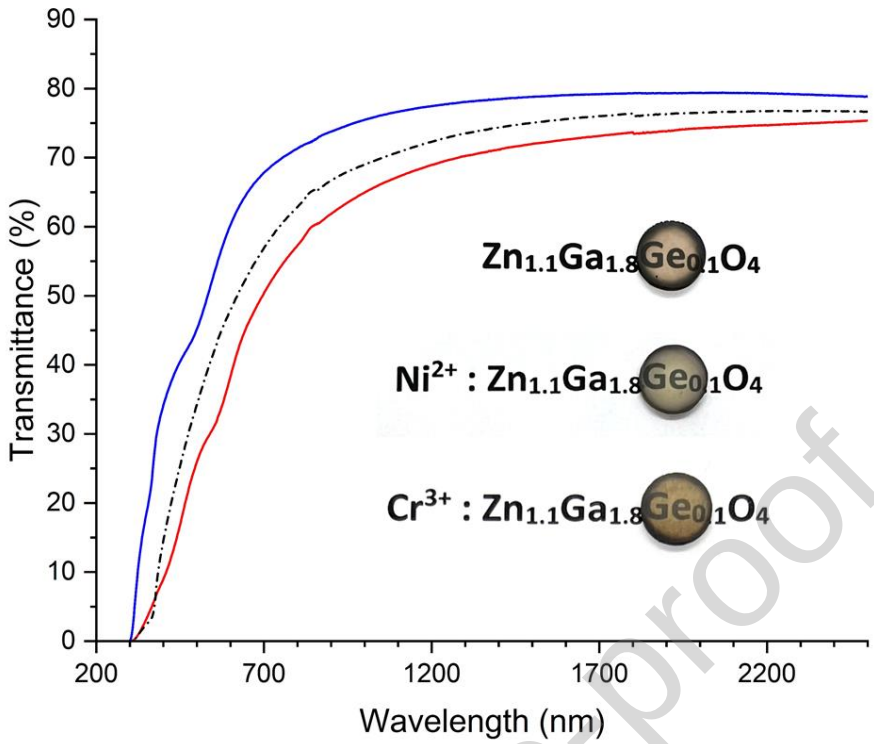

Figure SI-6: Transmission spectra measured through 1.15 mm thick samples for undoped $Zn_{1.1}Ga_{1.8}Ge_{0.1}O_4$ ceramic (blue) and ceramics doped with 0.1% of Cr^{3+} (red) and 0.05% Ni^{2+} (dashed black). The photographs of corresponding ceramics are presented.

References

[1] A. Ikesue, Y.L. Aung, Ceramic laser materials, Nature Photonics 2(12) (2008) 721-727.
[2] T. Benitez, S. Y. Gómez, A.P.N. de Oliveira, N. Travitzky, D. Hotza, Transparent ceramic and glass-ceramic materials for armor applications, Ceram. Int. 43(16) (2017) 13031-13046.
[3] G.R. Durand, Q. Bizot, N. Herbert, S. Quéméré, M. Pasturel, X.-H. Zhang, O. Merdrignac-Conanec, Processing of $CaLa_2S_4$ infrared transparent ceramics: A comparative study of HP and FAST/SPS techniques, J. Am. Ceram. Soc. 103(4) (2020) 2328-2339.
[4] A. Goldstein, A. Krell, Transparent Ceramics at 50: Progress Made and Further Prospects, J. Am. Ceram. Soc. (2016) 1-25.
[5] S. Tanaka, T. Takahashi, K. Uematsu, Fabrication of transparent crystal-oriented polycrystalline strontium barium niobate ceramics for electro-optical application, J. Eur. Ceram. Soc. 34(15) (2014) 3723-3728.
[6] A.D. Dupuy, Y. Kodera, J.E. Garay, Unprecedented Electro-Optic Performance in Lead-Free Transparent Ceramics, Adv. Mater. 28(36) (2016) 7970-7977.
[7] U. Peuchert, Y. Okano, Y. Menke, S. Reichel, A. Ikesue, Transparent cubic-ZrO_2 ceramics for application as optical lenses, J. Eur. Ceram. Soc. 29(2) (2009) 283-291.
[8] A. Bertrand, J. Carreaud, S. Chenu, M. Allix, E. Véron, J.-R. Duclère, Y. Launay, T. Hayakawa, C. Genevois, F. Brisset, F. Célarié, P. Thomas, G. Delaizir, Scalable and Formable Tellurite-Based Transparent Ceramics for Near Infrared Applications, Advanced Optical Materials 4(10) (2016) 1482-1486.
[9] N.J. Cherepy, J.D. Kuntz, Z.M. Seeley, S.E. Fisher, O.B. Drury, B.W. Sturm, T.A. Hurst, R.D. Sanner, J.J. Roberts, S.A. Payne, Transparent ceramic scintillators for gamma spectroscopy and radiography, SPIE 7805 (2010) 78050I-78050I.
[10] Z. Wang, G. Zhou, D. Jiang, S. Wang, Recent development of $A_2B_2O_7$ system transparent ceramics, Journal of Advanced Ceramics 7(4) (2018) 289-306.
[11] X. Ma, X. Li, J. Li, C. Genevois, B. Ma, A. Etienne, C. Wan, E. Véron, Z. Peng, M. Allix, Pressureless glass crystallization of transparent yttrium aluminum garnet-based nanoceramics, Nature Communications 9(1) (2018) 1175.

[12] S. Pimputkar, J.S. Speck, S.P. DenBaars, S. Nakamura, Prospects for LED lighting, Nature Photonics 3(4) (2009) 180-182.
[13] S. Maxim, R. Barak, K. Sergey, D.M. Peter, G. Ehud, F. Nachum, Transparent Polycrystalline Magnesium Aluminate Spinel Fabricated by Spark Plasma Sintering, Adv. Mater. 0(0) (2018) 1706283.
[14] J. Cheng, D. Agrawal, Y. Zhang, R. Roy, Microwave reactive sintering to fully transparent aluminum oxynitride (ALON) ceramics, J. Mater. Sci. Lett. 20(1) (2001) 77-79.
[15] L.B. Kong, Y.Z. Huang, W.X. Que, T.S. Zhang, S. Li, J. Zhang, Z.L. Dong, D.Y. Tang, Transparent Ceramics, Springer International Publishing2015.
[16] I. Milisavljevic, M.J. Pitcher, J. Li, S. Chenu, M. Allix, Y. Wu, Crystallization of glass materials into transparent optical ceramics, Int. Mater. Rev. (2022) 1-29.
[17] A. Krell, J. Klimke, T. Hutzler, Transparent compact ceramics: Inherent physical issues, Opt. Mater. 31(8) (2009) 1144-1150.
[18] Z.M. Seeley, J.D. Kuntz, N.J. Cherepy, S.A. Payne, Transparent Lu_2O_3:Eu ceramics by sinter and HIP optimization, Opt. Mater. 33(11) (2011) 1721-1726.
[19] G. Bonnefont, G. Fantozzi, S. Trombert, L. Bonneau, Fine-grained transparent $MgAl_2O_4$ spinel obtained by spark plasma sintering of commercially available nanopowders, Ceram. Int. 38(1) (2012) 131-140.
[20] K. Itatani, T. Tsujimoto, A. Kishimoto, Thermal and optical properties of transparent magnesium oxide ceramics fabricated by post hot-isostatic pressing, J. Eur. Ceram. Soc. 26(4) (2006) 639-645.
[21] L. An, A. Ito, T. Goto, Fabrication of transparent Lu_3NbO_7 by spark plasma sintering, Mater. Lett. 65(19–20) (2011) 3167-3169.
[22] M. Dolhen, J. Carreaud, G. Delaizir, J.-R. Duclère, M. Vandenhende, N. Tessier-Doyen, O. Tantot, D. Passerieux, P.-E. Coulon, P. Thomas, M. Allix, S. Chenu, New $KNbTeO_6$ transparent tellurate ceramics, J. Eur. Ceram. Soc. 40(12) (2020) 4164-4170.
[23] P. Aballea, A. Suganuma, F. Druon, J. Hostalrich, P. Georges, P. Gredin, M. Mortier, Laser performance of diode-pumped Yb:CaF_2 optical ceramics synthesized using an energy-efficient process, Optica 2(4) (2015) 288-291.
[24] R. Apetz, M.P.B. van Bruggen, Transparent alumina: A light-scattering model, J. Am. Ceram. Soc. 86(3) (2003) 480-486.
[25] H. Furuse, N. Horiuchi, B.-N. Kim, Transparent non-cubic laser ceramics with fine microstructure, Scientific Reports 9(1) (2019) 10300.
[26] Y. Sato, J. Akiyama, T. Taira, Orientation control of micro-domains in anisotropic laser ceramics, Opt. Mater. Express 3(6) (2013) 829-841.
[27] A. Ikesue, Y.L. Aung, Anisotropic alumina ceramics with isotropic optical properties, Journal of Advanced Ceramics 12(1) (2023) 72-81.
[28] G. Zhang, I. Milisavljevic, K. Grzeszkiewicz, P. Stachowiak, D. Hreniak, Y. Wu, New optical ceramics: High-entropy sesquioxide X_2O_3 multi-wavelength emission phosphor transparent ceramics, J. Eur. Ceram. Soc. (2021).
[29] X. Ming, F. Liu, Y. Chen, M. Chen, Y. Zhang, B. Liu, X. Wang, Z. Sun, R. Pan, K. Zheng, Y. Dai, Z. Deng, X. He, W. Cao, S. Wang, L. Wang, Elasto-Optic Effect of Lanthanum-Modified Lead Zirconate–Lead Titanate Transparent Ceramics: Application in Optical-Stress Sensors, Advanced Optical Materials 10(20) (2022) 2201239.
[30] R.J. Hill, J.R. Craig, G.V. Gibbs, Systematics of the spinel structure type, Phys. Chem. Miner. 4(4) (1979) 317-339.
[31] M. Rubat du Merac, H.-J. Kleebe, M.M. Müller, I.E. Reimanis, Fifty Years of Research and Development Coming to Fruition; Unraveling the Complex Interactions during Processing of $MgAl_2O_4$ Spinel, J. Am. Ceram. Soc. 96(11) (2013) 3341-3365.
[32] H. Wang, L.Y. Liu, P. Ye, Z. Huang, A.Y.R. Ng, Z. Du, Z. Dong, D. Tang, C.L. Gan, 3D Printing of Transparent Spinel Ceramics with Transmittance Approaching the Theoretical Limit, Adv. Mater. 33(15) (2021) 2007072.
[33] A. Goldstein, Y. Yeshurun, M. Vulfson, H. Kravits, Fabrication of Transparent Polycrystalline $ZnAl_2O_4$ – A New Optical Bulk Ceramic, J. Am. Ceram. Soc. 95(3) (2012) 879-882.
[34] X. Zong, H. Wang, H. Gu, L. Ren, B. Tu, W. Wang, S. Liu, Z. Fu, A novel spinel-type $Mg_{0.55}Al_{2.36}O_{3.81}N_{0.19}$ transparent ceramic with infrared transmittance range comparable to c-plane sapphire, Scripta Mater. 178 (2020) 428-432.
[35] G. Zhang, A. Goldstein, Y. Wu, Novel transparent $MgGa_2O_4$ and Ni^{2+}-doped $MgGa_2O_4$ ceramics, Journal of Advanced Ceramics 11(3) (2022) 470-481.
[36] C. Mével, J. Carreaud, G. Delaizir, J.-R. Duclère, F. Brisset, J. Bourret, P. Carles, C. Genevois, M. Allix, S. Chenu, First $ZnGa_2O_4$ Transparent Ceramics, J. Eur. Ceram. Soc. 41(9) (2021) 4934-4941.
[37] B. Wang, H. Wang, B. Tu, K. Zheng, H. Gu, W. Wang, Z. Fu, Optical transmission, dispersion, and transition behavior of $ZnGa_2O_4$ transparent ceramic, J. Am. Ceram. Soc. 106(2) (2022) 1-10.
[38] B. Wang, H. Wang, B. Tu, P. Xu, W. Wang, Z. Fu, Theoretical insight into optical properties of $ZnGa_2O_4$ transparent ceramic, Materials Today Communications (2023) 104846.
[39] Q. Liu, X. Mao, X. Li, P. Chen, X. Liu, Z. Liu, D. Zhu, H. Chen, T. Xie, J. Li, Fabrication and characterizations of Cr^{3+} doped $ZnGa_2O_4$ transparent ceramics with persistent luminescence, J. Am. Ceram. Soc. n/a(n/a) (2021).

[40] B. Wang, H. Wang, B. Chen, P. Xu, Q. Chen, B. Tu, W. Wang, Z. Fu, A novel durable spinel-type $ZnGa_2O_4$ transparent ceramic with wide transmission range, Scripta Mater. 205 (2021) 114186.
[41] S. Lyu, P. Zhou, J. Du, X. Wang, T. Wang, P. Wang, H. Wang, S. Sun, H. Lin, Manipulating trap distribution and density by chemical unit cosubstitution for near-infrared persistent luminescent $Zn_{1-2x}Li_xGa_{2+x}O_4:Cr^{3+}$ solid solutions, Journal of Materials Chemistry C (2022).
[42] M. Allix, S. Chenu, E. Véron, T. Poumeyrol, E.A. Kouadri-Boudjelthia, S. Alahraché, F. Porcher, D. Massiot, F. Fayon, Considerable Improvement of Long-Persistent Luminescence in Germanium and Tin Substituted $ZnGa_2O_4$, Chem. Mater. 25(9) (2013) 1600-1606.
[43] Y. Xiong, H. Xie, Z. Rao, L. Liu, Z. Wang, C. Li, Compositional modulation in $ZnGa_2O_4$ via Zn^{2+}/Ge^{4+} co-doping to simultaneously lower sintering temperature and improve microwave dielectric properties, Journal of Advanced Ceramics 10 (2021).
[44] H.M. Rietveld, A profile refinement method for nuclear and magnetic structures, J. Appl. Crystallogr. 2(2) (1969) 65-71.
[45] V. Petricek, M. Dusek, L. Palatinus, Crystallographic Computing System JANA2006: General features, Zeitschrift für Kristallographie. Crystalline materials 229(5) (2014) 345-352.
[46] C.A. Schneider, W.S. Rasband, K.W. Eliceiri, NIH Image to ImageJ: 25 years of image analysis, Nature Methods 9(7) (2012) 671-675.
[47] A. Degiovanni, Diffusivité et méthode flash, Rev. Gen. Therm. 185 (1977) 420-441.
[48] K. Morita, B.N. Kim, K. Hiraga, H. Yoshida, Fabrication of transparent $MgAl_2O_4$ spinel polycrystal by spark plasma sintering processing, Scripta Mater. 58(12) (2008) 1114-1117.
[49] S. Grasso, Y. Sakka, G. Maizza, Electric current activated/assisted sintering (ECAS): a review of patents 1906–2008, Science and Technology of Advanced Materials 10(5) (2009) 053001.
[50] D.S. Smith, F. Puech, B. Nait-Ali, A. Alzina, S. Honda, Grain boundary thermal resistance and finite grain size effects for heat conduction through porous polycrystalline alumina, Int. J. Heat Mass Transfer 121 (2018) 1273-1280.
[51] A. Bessiere, S. Jacquart, K. Priolkar, A. Lecointre, B. Viana, D. Gourier, $ZnGa_2O_4:Cr^{3+}$: a new red long-lasting phosphor with high brightness, Opt. Express 19(11) (2011) 10131-10137.
[52] W.W. Zhang, J.Y. Zhang, Z.Y. Chen, T.M. Wang, S.K. Zheng, Spectrum designation and effect of Al substitution on the luminescence of Cr^{3+} doped $ZnGa_2O_4$ nano-sized phosphors, J. Lumin. 130(10) (2010) 1738-1743.
[53] W. Mikenda, A. Preisinger, N-lines in the luminescence spectra of Cr^{3+} doped spinels. (II) Origins of N-lines, J. Lumin. 26(1-2) (1981) 67-83.
[54] J. Derkosch, W. Mikenda, N-lines in the luminescence spectra of Cr^{3+} doped spinels. (IV) Excitation spectra, J. Lumin. 28(4) (1983) 431-441.
[55] W. Nie, F.M. Michelcalendini, C. Linares, G. Boulon, C. Daul, New results on optical properties and term energy calculations in Cr^{3+} doped $ZnAl_2O_4$., J. Lumin. 46(3) (1990) 177-190.
[56] H.-J. Byun, J.-U. Kim, H. Yang, Blue, green, and red emission from undoped and doped $ZnGa_2O_4$ colloidal nanocrystals, Nanotechnology 20(49) (2009) 495602.
[57] S. Itoh, H. Toki, Y. Sato, K. Morimoto, T. Kishino, The $ZnGa_2O_4$ phosphor for low-voltage blue cathodoluminescence, J. Electrochem. Soc. 138(5) (1991) 1509-1512.
[58] C. Zhang, C. Li, J. Yang, Z. Cheng, Z. Hou, Y. Fan, J. Lin, Tunable Luminescence in Monodisperse Zirconia Spheres, Langmuir 25(12) (2009) 7078-7083.
[59] Z. Gao, Y. Liu, J. Ren, Z. Fang, X. Lu, E. Lewis, G. Farrell, J. Yang, P. Wang, Selective doping of Ni^{2+} in highly transparent glass-ceramics containing nano-spinels $ZnGa_2O_4$ and $Zn_{(1+x)}Ga_{(2-2x)}Ge_xO_4$ for broadband near-infrared fiber amplifiers, Scientific Reports 7 (2017) 1783.
[60] S. Chenu, E. Véron, C. Genevois, G. Matzen, T. Cardinal, A. Etienne, D. Massiot, M. Allix, Tuneable Nanostructuring of Highly Transparent Zinc Gallogermanate Glasses and Glass-Ceramics, Advanced Optical Materials 2(4) (2014) 364-372.
[61] M. Jin, F. Li, J. Xiahou, L. Zhu, Q. Zhu, J.-G. Li, A new persistent luminescence phosphor of $ZnGa_2O_4:Ni^{2+}$ for the second near-infrared transparency window, J. Alloys Compd. 931 (2023) 167491.
[62] A. Jouini, A. Yoshikawa, A. Brenier, T. Fukuda, G. Boulon, Optical properties of transition metal ion-doped $MgAl_2O_4$ spinel for laser application, physica status solidi (c) 4 (2007) 1380-1383.
[63] Y. Abe, D.E. Clark, Determination of combined water in glasses by infrared spectroscopy, J. Mater. Sci. Lett. 9(2) (1990) 244-245.

Declaration of interests

☒ The authors declare that they have no known competing financial interests or personal relationships that could have appeared to influence the work reported in this paper.

☐The authors declare the following financial interests/personal relationships which may be considered as potential competing interests: